Miniature cavity-enhanced diamond magnetometer

Georgios Chatzidrosos,[1, a)] Arne Wickenbrock,[1] Lykourgos Bougas,[1] Nathan Leefer,[1] Teng Wu,[1] Kasper Jensen,[2] Yannick Dumeige,[3] and Dmitry Budker[1, 4, 5, 6]

[1)] *Johannes Gutenberg-Universität Mainz, 55128 Mainz, Germany*

[2)] *Niels Bohr Institute, University of Copenhagen, Blegdamsvej 17, 2100 Copenhagen, Denmark*

[3)] *CNRS, UMR 6082 FOTON, Enssat, 6 rue de Kerampont, CS 80518, 22305 Lannion cedex, France*

[4)] *Helmholtz Institut Mainz, 55099 Mainz, Germany*

[5)] *Department of Physics, University of California, Berkeley, CA 94720-7300, USA*

[6)] *Nuclear Science Division, Lawrence Berkeley National Laboratory, Berkeley, CA 94720, USA*

We present a highly sensitive miniaturized cavity-enhanced room-temperature magnetic-field sensor based on nitrogen-vacancy (NV) centers in diamond. The magnetic resonance signal is detected by probing absorption on the 1042 nm spin-singlet transition. To improve the absorptive signal the diamond is placed in an optical resonator. The device has a magnetic-field sensitivity of $28\,\mathrm{pT}/\sqrt{\mathrm{Hz}}$, a projected photon shot-noise-limited sensitivity of $22\,\mathrm{pT}/\sqrt{\mathrm{Hz}}$ and an estimated quantum projection-noise-limited sensitivity of $0.43\,\mathrm{pT}/\sqrt{\mathrm{Hz}}$ with the sensing volume of $\sim 390\,\mu\mathrm{m} \times 4500\,\mu\mathrm{m}^2$. The presented miniaturized device is the basis for an endoscopic magnetic field sensor for biomedical applications.

INTRODUCTION

Biomagnetic signatures are an important diagnostic tool to understand the underlying biological processes. Time-resolved biomagnetic signals are measured with Hall probes[1], Giant magnetoresistance sensors[2], alkali-vapor magnetometers[3], superconducting quantum interference devices (SQUIDs)[4] and single negatively-charged nitrogen-vacancy (NV) centers or ensembles thereof[5]. Typical devices probe magnetic fields outside the body, i.e., far from their origin. However, signal strength and spatial resolution can both be improved by utilizing endoscopic sensors. The most sensitive from the above magnetometers are based on SQUIDs and alkali-vapor cells, but neither is ideal for biological applications.

NV centers in diamond have already been used as nanoscale-resolution sensors [6–8] with high sensitivity [5,9]. Prominent examples of sensing with NV centers include, single neuron-action potential detection [5], single protein spectroscopy [10], as well as in vivo thermometry [11]. Due to their ability to operate in a wide temperature range as well as their small size, NV magnetometers are amenable for in-vivo and/or endoscopic applications.

The majority of NV sensors use a photoluminescence (PL) detection which suffers from low photon-detection efficiency. Approaches to counter this problem include, for example, the use of solid immersion lenses[12–14], or employ infrared (IR) absorption[15–17]. Compared to NV sensors based on PL detection, those based on absorption feature collection efficiency approaching unity[16].

Due to the small cross-section of the IR transition [15,16], to achieve similar or higher sensitivities compared to PL-detection techniques, we use an optical cavity to enhance the optical pathlength in the diamond, and thus the IR absorption signal [15,17]. With the cavity enhancement we can achieve sensitivities closer to the fundamental projection-noise limit, even at room temperature[15,17].

Here we demonstrate a sensitive compact cavity-based IR absorption device operating near the photon shot-noise limit opening realistic prospects for a practical endoscopic magnetometer. The best DC magnetometer using NV centers, in a sensing volume of 13 × 200 × 2000 $\mu\mathrm{m}^3$, have reached magnetic field sensitivity of $15(1)\,\mathrm{pT}/\sqrt{\mathrm{Hz}}$ (Ref. 5). Our sensor features a similar sensing volume and sufficient sensitivity to measure biomagnetic signals e.g. magnetic signals by the human heart.

EXPERIMENT

The ground and excited electronic spin-triplet states of NV are $^3\mathrm{A}_2$ and $^3\mathrm{E}$, respectively [Fig. 1 (a)], with the transition between them having a zero-phonon line at 637 nm. The lower and upper electronic singlet states are $^1\mathrm{E}$ and $^1\mathrm{A}_1$, respectively, with the transition between them having a zero-phonon line at 1042 nm (IR). While optical transition rates are spin-independent, the probability of nonradiative intersystem crossing from $^3\mathrm{E}$ to the singlets is several times higher[15] for $m_s = \pm 1$ than that for $m_s = 0$. As a consequence, under continuous illumination with green pump light (532 nm), NV centers are prepared in the $^3\mathrm{A}_2$ $m_s = 0$ ground state sublevel and in the metastable $^1\mathrm{E}$ singlet state. For metrology applications, the spins in the the $^3\mathrm{A}_2$ ground state can be coherently manipulated by microwave fields. In this

[a)] Electronic mail: gechatzi@uni-mainz.de

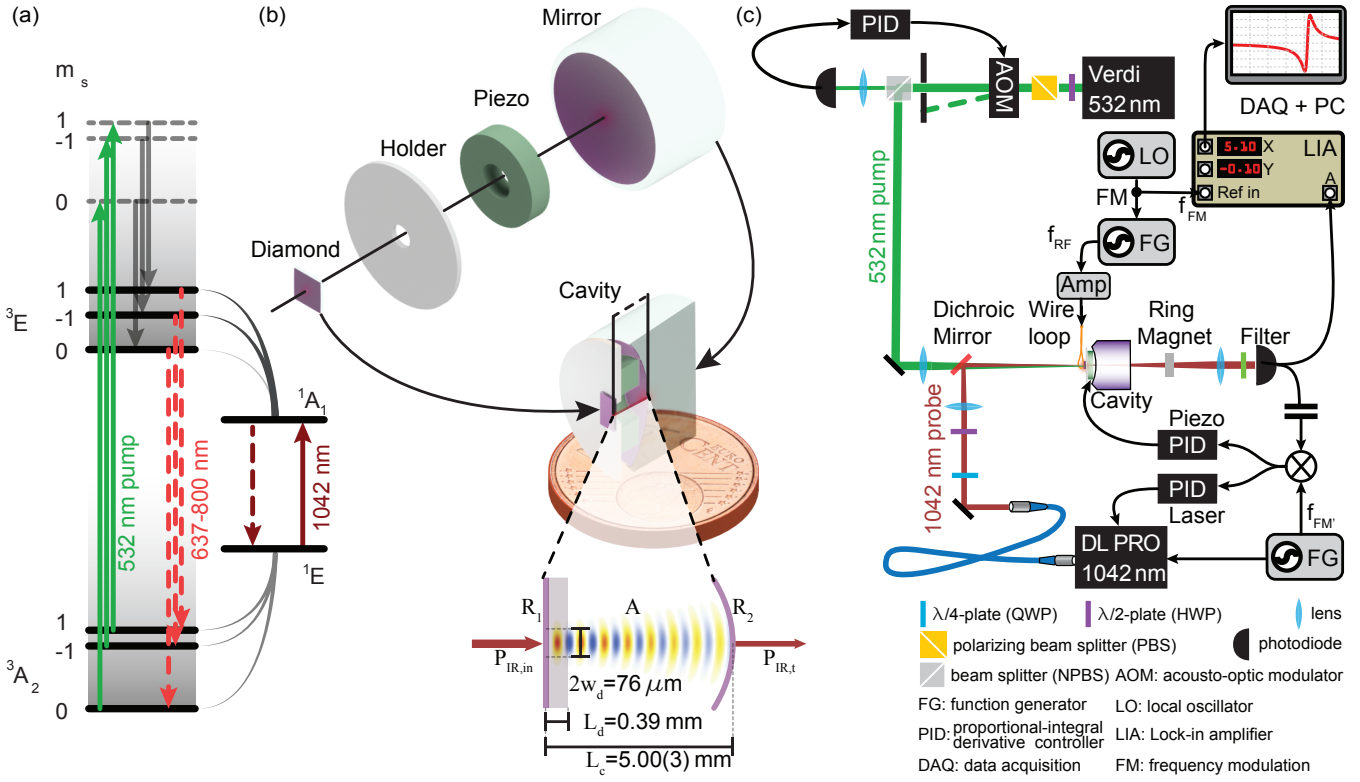

FIG. 1. (a) Relevant NV center energy levels and transitions (Ref. 5). Solid green and red lines indicate excitations, dashed lines indicate radiative transitions, and gray solid lines indicate non-radiative transitions. (b) Explosion view and 2D cross section of the cavity magnetometer (c) Schematic of the experimental setup.

work, the population of the ground state is inferred by monitoring IR light absorption on the singlet transiton.

The diamond sample used for this sensor is a type Ib, (111)-cut, HPHT grown sample, purchased from Element Six. The initial nitrogen concentration of the sample was specified as < 100 ppm, which seems consistent with linewidth measurements. The sample was irradiated with 5 MeV electrons and dosage of $2 \times 10^{19}\,\mathrm{cm}^{-2}$ and then annealed at 700 ^{o}C for 2 hours.

To increase the absorption of IR light we construct a cavity as shown in Fig. 1 (b). A spherical mirror with a curvature radius of 10 mm, reflectivity $R_2 = 99.2(8)\%$ (see supplemental material[18]) and diameter of 12.5 mm serves as the output mirror. A piezoelectric transducer is used to adjust the length of the cavity within a range of a few μm. It is glued with an epoxy resin (Torr Seal) between the spherical mirror and the ceramic holder for the diamond. The diamond plate serves as the input plane mirror of the cavity and is glued to the holder. The holder doubles as a heat sink. The (111)-cut diamond plate is dielectrically coated with high reflectivity $R_1 \sim 98.5\%$ for IR light as well as anti-reflective for green light on the outside of the cavity. The diamond surface inside the cavity is supplied with an anti-reflective coating for both green light and IR light. The reflectivity of the coatings for both, the diamond and the output mirror, were chosen according to the losses in the diamond. The total optical length of the cavity is $L_c = 5.00(3)$ mm, and the finesse is $\mathscr{F} = 160(4)$ (see supplemental material[18]). The cavity mode has a waist on the diamond with a radius of $w_d = 38\,\mu$m; the mode radius is $54\,\mu$m on the concave mirror surface. With this design, it is possible to bring the diamond's outer surface in close proximity to a magnetic sample under study in compact geometry. Currently, the diameter of our sensor is 12.5 mm with a total length of ~ 8 mm. For comparison, some modern medical endoscopes feature comparable outer diameters (Olympus, GIF-2TH180, 12.6 mm).

The setup for magnetometric measurements is shown in Fig. 1 (c). Green light is provided by a diode-pumped solid-state laser (Coherent, Verdi V10) and IR light is provided by an external-cavity diode laser (ECDL, Toptica DL-Pro). The green laser power is stabilized using an acousto-optical modulator (AOM, ISOMET-1260C with an ISOMET 630C-350 driver) controlled through a proportional-integral-derivative controller (PID, SIM960). The IR beam profile is matched to the lowest-order transversal cavity mode (TEM_{00}), while the green beam is overlapped with the IR beam in the diamond; the green beam profile does not have to be mode matched to the cavity but it should be bigger than the IR profile to provide a homogeneous pumping rate of the interrogated NV centers. The frequency difference of the laser and the cavity mode is stabilized using an

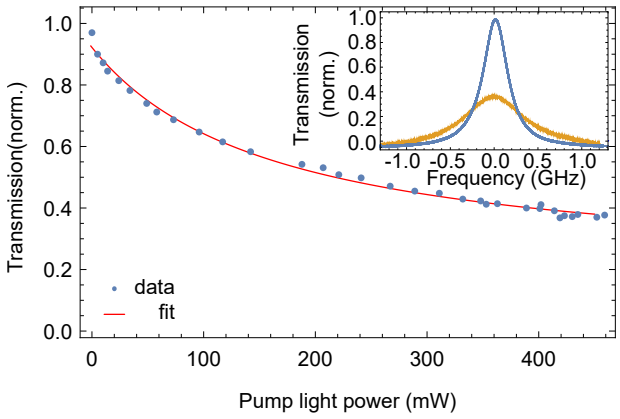

FIG. 2. IR light transmission of the cavity ($P_{IR,t}$ as a function of green pump power (P_{532}). The transmission is normalized to unity for zero pump power. The inset displays the TEM_{00} cavity mode at 0 mW (blue) and 500 mW of pump light power (amber) .

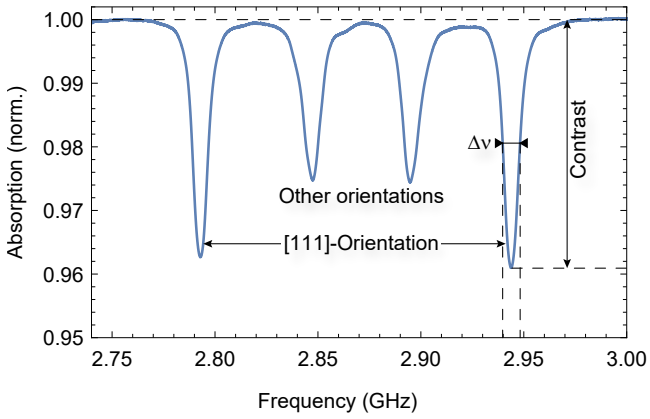

FIG. 3. IR transmission signal normalized to unity off resonance as a function of microwave frequency.

error signal derived by frequency modulation of the laser ($f_{FM'}$=2.4 MHz). Two PIDs are deployed for the feedback. One to lock the cavity piezo to the laser (bandwidth 6 kHz) and the other to provide feedback to the laser controller. The latter addresses piezo and current of the ECDL and has a bandwidth of 21 kHz.

The microwaves (MW) to manipulate the NV spins are generated by a MW generator (SRS SG394). They are amplified with a 16 W amplifier (ZHL-16W-43+), passed through a circulator (CS-3.000, not shown in Fig.1) and high-pass filtered (Mini Circuits VHP-9R5), before they are applied to the NV centers using a mm-sized wire loop. The other side of the wire is directly connected to ground. A bias magnetic field is applied with a permanent ring magnet mounted on a precision positioning stage.

RESULTS AND DISCUSSION

The cavity transmission signal $P_{IR,t}$ for IR light is shown in Fig. 2 as a function of green light power P_{532} in front of the cavity. The steady-state population of the singlet state increases with increasing green power, resulting in higher IR absorption. The IR absorption is enhanced by the cavity by $2\mathscr{F}/\pi$, yielding significantly reduced IR transmission for higher pump powers. Higher absorption also results in an increase of the cavity-mode linewidth (Fig. 2, inset). The data in Fig. 2 are fitted with a saturation curve $P_{IR,t}(P_{532})/P_{IR,t}(P_{532} = 0) = 1 - \alpha P_{532}/(P_{532} + P_{532,sat})$ (Ref.17), with saturation power $P_{532,sat}$ and reduction in transmission at saturation α. The fit results are $P_{532,sat} = 735(1)$ mW and $\alpha = 0.605(1)$. Magnetic-resonance measurements (Fig. 3) are performed by scanning the MW frequency around the NV zero-field splitting (2.87 GHz). When the MW field is resonant with the ground-state $m_s = 0 \rightarrow m_s = \pm 1$ transitions, population is transferred through the exited triplet state to the metastable singlet state, resulting in increased IR absorption, which produces the observed optically detected magnetic resonance (ODMR) signal.

With a bias magnetic field (in this case, about 3 mT) aligned along the [111] axis, four peaks are visible by scanning the MW frequency (Fig. 3). The outer features result from the NVs along the [111] axis and the inner features from the remaining NV orientations. The relative amplitudes of ODMR peaks depend on several things, such as, polarization of MWs, IR light polarization and green light polarization. It will also depend on how well the magnetic field is aligned, as if it is not perfectly along [111]-direction, the innermost peaks will broaden and have reduced amplitude The contrast $\mathscr{C}$ and the full width at half maximum $\Delta\nu$ of the outer peaks are $\sim 3.7\,\%$ and 5.6 MHz, respectively.

For the magnetometric measurements we focus on the highest frequency feature in Fig. 3. We modulate the MW frequency f_{MW} around the central frequency f_c of the feature with frequency $f_{mod} = 8.6$ kHz and amplitude $f_{dev} = 4.5$ MHz: $f_{MW} = f_c + f_{dev}\cos(2\pi f_{mod} t)$ and detect the first harmonic of the transmission signal with a lock-in amplifier (LIA). These values were chosen to optimize the sensors noise floor in the laboratory environment. Fig. 4 shows the resulting dispersive signal centered at the feature (red) along with the feature itself (blue). Around the zero-crossing of the dispersive feature, we observe a linear signal $S_{LI} \sim a(f_c - f_{res})$ as a function of $(f_c - f_{res})$ when $|f_c - f_{res}| << \Delta\nu/2$. We extract the slope $a \propto \mathscr{C}/\Delta\nu$ from the fit of Fig. 4 (black) and use it to convert the magnetometer's voltage output into magnetic field.

Figure 5 shows the magnetic-field-noise spectrum. The spectrum was obtained by a Fourier transform of the LIA output with a reference frequency of 8.6 kHz. The peaks at 50 Hz and harmonics are attributed to magnetic field from the power line in the lab and are not visible on the magnetically insensitive spectrum, which we ob-

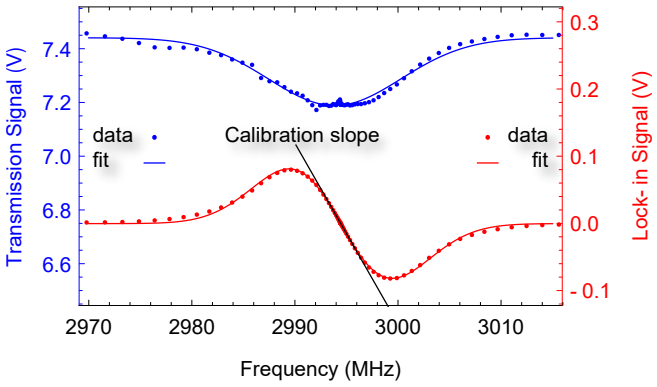

FIG. 4. The cavity-transmission signal (blue) and lock-in demodulated signal (red) as a function of a central frequency f_c scanned over a magnetic resonance. The experimental data are represented with dots and the fits with solid lines. The slope of the fit is represented with a straight line.

tain in the absence of a MW field. The noise floor in the region of 60-90 Hz for the magnetically insensitive spectrum is calculated as $28\,\mathrm{pT}/\sqrt{\mathrm{Hz}}$. The above measurements where obtained at 400 mW of pump light and 80 mW of IR which was the maximum available for our system.

This sensitivity is ≈ 100 times better than what has been demonstrated previously with magnetometers based on IR absorption[17]. The photon-shot-noise limited sensitivity of the two sensors is comparable ($70\,\mathrm{pT}/\sqrt{\mathrm{Hz}}$ against $22\,\mathrm{pT}/\sqrt{\mathrm{Hz}}$) using similar sensing volumes, while the length of the cavity was reduced by an order of magnitude. Main improvements that aided in the increased sensitivity are: a dramatic reduction in cavity size, increase in probe laser power and improvements to the laser-lock stability. The size reduction translates to robustness in frequency noise of the laser. The increase in IR light power allowed us to surpass the shot-noise-limit of the previous design. While with improvements to the laser-lock stability we were able to optimize the sensor's noise-floor in regards to the noise of the laboratory. We verify the sensitivity by applying test magnetic fields (see supplemental material[18]). The photon shot noise limit is estimated as $22\,\mathrm{pT}/\sqrt{\mathrm{Hz}}$ for 4.2 mW of collected IR light. The electronic shot noise is $2\,\mathrm{pT}/\sqrt{\mathrm{Hz}}$. For an estimated NV density in the metastable singlet state of 0.68(1) ppm (see supplemental material[18]) and the demonstrated ODMR linewidth $\Delta\nu = 5.6$ MHz we calculate a spin-projection noise limit of $0.43\,\mathrm{pT}/\sqrt{\mathrm{Hz}}$. The bandwidth of the magnetometer is set by the LIA filter settings. For the presented measurements a time constant of 300 μs results in a 530 Hz bandwidth. The filter steepness is selected as 24dB/octave.

We demonstrate a miniaturized cavity-enhanced room-temperature absorption-based magnetometer using NV centers in diamond. The small size of our magnetometer yields a robust device with improved magnetic field sensitivity and makes it an ideal candidate for endoscopic measurements. The closer proximity to biomagnetic signal sources, inherent to endoscopic measurements, provides enhanced signal strength and spatial resolution, which may be further improved by using a combination of a different diamond with narrower ODMR feature linewidth and a higher finesse cavity. To realize the endoscopic sensor design the following changes must be made; The diamond should act as the output mirror of the cavity, an all optical protocol has to implemented, the two different light beams should be delivered by an optical fiber and smaller components (e.g. mirror) have to used when possible. With the diamond acting as the output mirror we would have better access to the surface of the diamond sensor, the sensor would then detect the signal on reflection rather than transmission allowing samples to be placed close to the diamond plate without blocking any of the light sources. An all optical protocol as in Ref. 19 would allow us to avoid the usage of MW which could be detrimental for biomedical applications. If we deliver the light beams with an optical fiber we could reduce the need for extra optical components and reduce the footprint of our sensor. Smaller components, such as a smaller mirror and diamond, should also be used in the next design for the same purpose.

Our sensor features a noise-floor of $28\,\mathrm{pT}/\sqrt{\mathrm{Hz}}$ close to the shot-noise limit (see supplemental material[18]). The sensitivity may be improved in future iterations by increasing the IR light power[20], optimizing the impedance matching condition of the cavity[15] to provide higher contrast, implementing AC sensing protocols that allow increased NV coherence times due to dynamic decoupling from the decoherence sources[21], and using a diamond sample with narrower linewidth which would increase the calibration slope obtained by the calculation of Fig. 4.

ACKNOWLEDGMENTS

The authors acknowledge support by the German Federal Ministry of Education and Research (BMBF) within the Quantumtechnologien program (FKZ 13N14439) and the DFG through the DIP program (FO 703/2-1). GC acknowledges support by the internal funding of JGU. NL acknowledges support from a Marie Curie International Incoming Fellowship within the 7th European Community Framework Programme. LB is supported by a Marie Curie Individual Fellowship within the second Horizon 2020 Work Programme. DB acknowledges support from the AFOSR/DARPA QuASAR program. We thank J.W. Blanchard for a fruitful discussion.

REFERENCES

[1] P. Manandhar, K.-S. Chen, K. Aledealat, G. Mihajlovi, C. S. Yun, M. F., G. J. Sullivan, G. F. S., P. B. Chase, S. von Molnr,

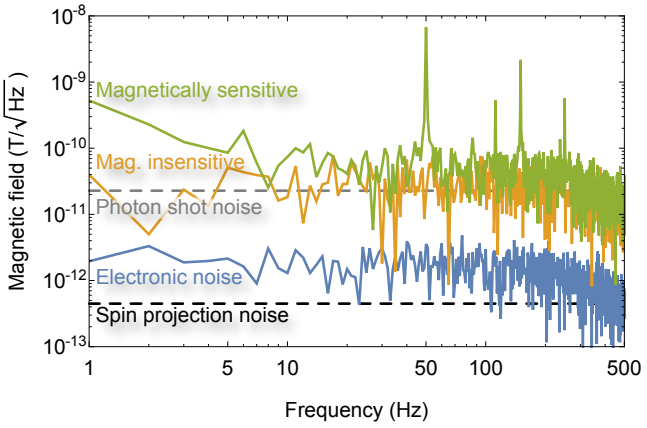

FIG. 5. Magnetic-field noise spectrum (green) represents the magnetically sensitive spectrum corresponding to a environment limited noise floor of $37\,\mathrm{pT}/\sqrt{\mathrm{Hz}}$ between 60 and 90 Hz, (amber) the magnetically insensitive with a noise floor of $28\,\mathrm{pT}/\sqrt{\mathrm{Hz}}$ and (blue) the electronic noise with a floor of $2\,\mathrm{pT}/\sqrt{\mathrm{Hz}}$. The shot noise limit of the system and the spin projection noise are also depicted with a dashed lines at $22\,\mathrm{pT}/\sqrt{\mathrm{Hz}}$ and $0.43\,\mathrm{pT}/\sqrt{\mathrm{Hz}}$, respectively.

and P. Xiong, "The detection of specific biomolecular interactions with micro-hall magnetic sensors," *Nanotechnology*, vol. 20, no. 35, p. 355501, 2009.

[2]F. Barbieri, V. Trauchessec, L. Caruso, J. Trejo-Rosillo, B. Telenczuk, E. Paul, T. Bal, A. Destexhe, C. Fermon, M. Pannetier-Lecoeur, and G. Ouanounou, "Local recording of biological magnetic fields using giant magneto resistance-based micro-probes," *Scientific Reports*, vol. 6, no. 39330, p. 39330, 2016.

[3]K. Jensen, R. Budvytyte, R. A. Thomas, T. Wang, A. M. Fuchs, M. V. Balabas, G. Vasilakis, L. D. Mosgaard, H. C. Stærkind, J. H. Müller, T. Heimburg, S.-P. Olesen, and E. S. Polzik, "A protease-based biosensor for the detection of schistosome cercariae," *Scientific Reports*, vol. 6, no. 24725.

[4]U. D. Ulusar, J. D. Wilson, P. Murphy, R. B. Govindan, H. Preissl, C. L. Lowery, and H. Eswaran, "Bio-magnetic signatures of fetal breathing movement," *Physiological Measurement*, vol. 32, no. 2, p. 263, 2011.

[5]J. F. Barry, M. J. Turner, J. M. Schloss, D. R. Glenn, Y. Song, M. D. Lukin, H. Park, and R. L. Walsworth, "Optical magnetic detection of single-neuron action potentials using quantum defects in diamond," *PNAS*, vol. 113, p. 14133, 2016.

[6]G. Balasubramanian, I. Y. Chan, R. Kolesov, M. Al-Hmoud, J. Tisler, C. Shin, C. Kim, A.Wojcik, P. R. Hemmer, A. Krueger, T. Hanke, A. Leitenstorfer, R. Bratschitsch, F. Jelezko, and J. Wrachtrup, "Nanoscale imaging magnetometry with diamond spins under ambient conditions," *Nature*, vol. 455, no. 7213, pp. 648–651, 2008.

[7]J. R. Maze, P. L. Stanwix, J. S. Hodges, S. Hong, J. M. Taylor, P. Cappellaro, L. Jiang, M. V. G. Dutt, E. Togan, A. S. Zibrov, A. Yacoby, R. L. Walsworth, and M. D. Lukin, "Nanoscale magnetic sensing with an individual electronic spin in diamond," *Nature*, vol. 455, no. 7213, pp. 644–647, 2008.

[8]E. Rittweger, K. Y. Han, S. E. Irvine, C. Eggeling, and S. W. Hell, "Sted microscopy reveals crystal colour centres with nanometric resolution," *Nat Photon*, vol. 3, no. 3, pp. 144–147, 2009.

[9]T. Wolf, P. Neumann, K. Nakamura, H. Sumiya, T. Ohshima, J. Isoya, and J. Wrachtrup, "Subpicotesla diamond magnetometry," *Phys. Rev. X*, vol. 5, p. 041001, Oct 2015.

[10]I. Lovchinsky, A. O. Sushkov, E. Urbach, N. P. de Leon, S. Choi, K. D. Greve, R. Evans, R. Gertner, E. Bersin, C. Müller, L. McGuinness, F. Jelezko, R. L. Walsworth, H. Park, and M. D. Lukin, "Nuclear magnetic resonance detection and spectroscopy of single proteins using quantum logic," *Science*, vol. 351, p. 836, 2016.

[11]G. Kucsko, P. C. Maurer, N. Y. Yao, M. Kubo, H. J. Noh, P. K. Lo, H. Park, and M. D. Lukin, "Nanometre-scale thermometry in a living cell," *Nature*, vol. 500, pp. 54–58, October 2013.

[12]J. P. Hadden, J. P. Harrison, A. C. Stanley-Clarke, L. Marseglia, Y.-L. D. Ho, B. R. Patton, J. L. OBrien, and J. G. Rarity, "Strongly enhanced photon collection from diamond defect centers under microfabricated integrated solid immersion lenses," *Applied Physics Letters*, vol. 97, no. 24, p. 241901, 2010.

[13]P. Siyushev, F. Kaiser, V. Jacques, I. Gerhardt, S. Bischof, H. Fedder, J. Dodson, M. Markham, D. Twitchen, F. Jelezko, and J. Wrachtrup, "Monolithic diamond optics for single photon detection," *Applied Physics Letters*, vol. 97, no. 24, p. 241902, 2010.

[14]D. Le Sage, L. M. Pham, N. Bar-Gill, C. Belthangady, M. D. Lukin, A. Yacoby, and R. L. Walsworth, "Efficient photon detection from color centers in a diamond optical waveguide," *Phys. Rev. B*, vol. 85, p. 121202, Mar 2012.

[15]Y. Dumeige, M. Chipaux, V. Jacques, F. Treussart, J.-F. Roch, T. Debuisschert, V. M. Acosta, A. Jarmola, K. Jensen, P. Kehayias, and D. Budker, "Magnetometry with nitrogen-vacancy ensembles in diamond based on infrared absorption in a doubly resonant optical cavity," *Phys. Rev. B*, vol. 87, p. 155202, Apr 2013.

[16]V. M. Acosta, E. Bauch, A. Jarmola, L. J. Zipp, M. P. Ledbetter, and D. Budker, "Broadband magnetometry by infrared-absorption detection of nitrogen-vacancy ensembles in diamond," *Applied Physics Letters*, vol. 97, no. 17, p. 174104, 2010.

[17]K. Jensen, N. Leefer, A. Jarmola, Y. Dumeige, V. M. Acosta, P. Kehayias, B. Patton, and D. Budker, "Cavity-enhanced room-temperature magnetometry using absorption by nitrogen-vacancy centers in diamond," *Phys. Rev. Lett.*, vol. 112, p. 160802, 2014.

[18]See Supplemental Material at [URL will be inserted by publisher].

[19]H. Zheng, G. Chatzidrosos, A. Wickenbrock, L. Bougas, R. Lazda, A. Berzins, F. H. Gahbauer, M. Auzinsh, R. Ferber, and D. Budker, "Level anti-crossing magnetometry with color centers in diamond," *Proc. SPIE*, vol. 10119, 2017.

[20]V. M. Acosta, A. Jarmola, E. Bauch, and D. Budker, "Optical properties of the nitrogen-vacancy singlet levels in diamond," *Phys. Rev. B*, vol. 82, p. 201202, 2010.

[21]D. Farfurnik, A. Jarmola, L. M. Pham, Z.-H. Wang, V. V. Dobrovitski, R. L. Walsworth, D. Budker, and N. Bar-Gill *Phys. Rev. B*, vol. 92, p. 060301, 2015.